Article of scientific research / *https://doi.org/10.15446/rcciquifa.v52n1.109381*

Molecular insights into the binding mechanisms of human and mouse Glutamate-cysteine ligases

Ige Olaoye[1,2], Babatunde Oso[1a*], Adepeju Aberuagba[1,2b*]

[1] Department of Biochemistry, McPherson University, Seriki Sotayo, Nigeria.

[2] Department of Biochemistry, University of Ilorin, Ilorin, Nigeria.

*Corresponding authors:

[a] Department of Biochemistry, McPherson University; Km 96, Lagos-Ibadan Express way, Nigeria; +2348060625697; E-mail: basjoe08@gmail.com; ORCID: https://orcid.org/0000-0001-8667-7108

[b] Department of Biochemistry, McPherson University; Km 96, Lagos-Ibadan Express way, Nigeria; +2348068017723; E-mail: adepaberuagba@gmail.com; ORCID: https://orcid.org/0000-0003-1055-1407

Received: March 31, 2022

Corrected: December 1, 2022

Accepted: December 6, 2022

Summary

Background: the significant role of glutamate-cysteine ligase (GCL) towards the synthesis of glutathione for the sequestration of reactive species as a regulatory point is second to none. However, much still need to be known about the enzyme molecular characterization. Thus, the homology modeling of GCL was carried out using different modeling webserver tools. The quality of the predicted crystal structures of human and mouse GCLs with inhibition were further assessed on molecular interaction with naphthalene and its metabolites. **Results:** the predicted human GCL and mouse GCL model structures have respective 89.8% and 89.6% residues in the most favored region of the Ramachandran plot. However, the molecular docking interaction study with the assessed ligands revealed two different binding pockets with pi-interactions as major non-covalent bond and better binding scores than glutathione. **Conclusion:** the predicted model could provide better mechanism of GCL catalysis to preserve its essential residues for reasonable GSH synthesis.

Keywords: GSH, GCL, homology modeling, naphthalene, molecular docking.

Resumen

Información molecular sobre los mecanismos de unión de las ligasas de glutamato-cisteína humana y de ratón

Antecedentes: el importante papel de la glutamato-cisteína ligasa (GCL) en la síntesis de glutatión para el secuestro de especies reactivas como punto regulador es insuperable. Sin embargo, aún queda mucho por conocer acerca de la caracterización molecular de enzimas. Por lo tanto, el modelado de homología de GCL se llevó a cabo utilizando diferentes herramientas de servidor web de modelado. La calidad de las estructuras cristalinas predichas de los GCL humanos y de ratón con inhibición se evaluó más a fondo en la interacción molecular con el naftaleno y sus metabolitos. **Resultados:** las estructuras del modelo de GCL humano y GCL de ratón predichas tienen residuos respectivos del 89,8 % y el 89,6 % en la región más favorecida del diagrama de Ramachandran. Sin embargo, el estudio de interacción de acoplamiento molecular con los ligandos evaluados reveló dos bolsillos de unión diferentes con interacciones pi como enlace no covalente principal y mejores puntajes de unión que el glutatión. **Conclusión:** el modelo predicho podría proporcionar un mejor mecanismo de catálisis de GCL para preservar sus residuos esenciales para una síntesis razonable de GSH.

Palabras clave: GSH, GCL, modelado por homología, naftalina, acoplamiento molecular.

Resumo

Insights moleculares sobre os mecanismos de ligação de ligases de glutamato-cisteína humanas e de camundongos

Antecedentes: o papel significativo da glutamato-cisteína ligase (GCL) para a síntese de glutationa para o sequestro de espécies reativas como um ponto regulador é inigualável. No entanto, muito ainda precisa ser conhecido sobre a caracterização molecular da enzima. Assim, a modelagem de homologia do GCL foi realizada usando diferentes ferramentas de modelagem do servidor web. A qualidade das estruturas cristalinas previstas de GCLs humanos e de camundongos com inibição foi ainda avaliada na interação molecular com naftaleno e seus metabólitos. **Resultados:** as estruturas do modelo de GCL humano e GCL de camundongo têm resíduos respectivos de 89,8% e 89,6% na região mais favorecida do gráfico de Ramachandran. No entanto, o estudo da interação de docking molecular com os ligantes

avaliados revelou dois bolsos de ligação diferentes com interações pi como principal ligação não covalente e melhores pontuações de ligação do que a glutationa. **Conclusão:** o modelo previsto pode fornecer um melhor mecanismo de catálise de GCL para preservar seus resíduos essenciais para síntese razoável de GSH.

Palavras-chave: GSH, GCL, modelagem de homologia, naftaleno, docking molecular.

Introduction

Glutathione (GSH) is a tripeptide (γ-glutamyl–cysteinyl–glycine) the most abundant non-protein thiol in the cell that is ubiquitously expressed as a cellular antioxidant to prevent the adverse effects of excessive ROS [1]. It is also a cofactor for GPXs and GSTs [2]. Glutamate-cysteine ligase-catalytic subunit, glutathione synthase, and glutathione reductase have been demonstrated to be responsible for the synthesis of GSH [3]. Sequential actions glutamate-cysteine ligase (GCL) (EC 6.3.2.2) and GSH synthetase (EC 6.3.2.3) is a synthetic pathway that occurs in nearly all cell types in mammals that mostly leads to the generation of GSH. The catalytic ability and expression of GCL gene have been found to correlate with GSH synthesis. GCL is a heterodimer enzyme composing of catalytically active heavy subunit and a light (modifier) subunits. The heavy subunit contains all substrate binding sites which catalyzes the rate limiting step in de novo synthesis of GSH [4, 5]. It catalyzes the formation of a peptidic γ-linkage between the γ-carboxyl group of glutamate and amino group of cysteine. GCL is an important antioxidative enzyme, which could function in the reduction of hydrogen and lipid peroxides, detoxification of toxic electrophiles, and maintenance of cellular redox status [6]. The control of the metabolic processes involving GCL depends on the regulation of enzymes activity which can be achieved by altering the rate of GCL synthesis, degradation, induction, repression and the catalytic efficiency of the enzyme through feedback inhibition and modulation of the affinity of the catalytic subunit for substrates and inhibitors through the regulatory light (modifier) subunit.

Various physiological disorders such viral infections and marked increase in oxidative stress have been shown to compromise glutathione synthesis in mammals as they correlate with decreased levels of cellular GSH [3, 7]. Environmental electrophilic chemicals such as aromatic hydrocarbons, quinones, and heavy metals can induce oxidative stress through formation of adducts with variety of biological nucleophiles such as GSH and proteins. They can also induce the activation of redox signal transduction pathways leading to changes in the expression and activity of GCL [8].

These electrophiles include naphthalene, an indoor air pollutant that generate reactive species from its bio-activation to highly cytotoxic epoxide such as 1R, 2S-naphthalene oxide by cytochrome P450s: CYP2F2 and CYP2F4 respectively [9].

This study discusses the homolog modeling vis-a-vis structural characterization of human and mouse Glutamate-cysteine ligases and their respective interaction with an environmental electrophile: naphthalene and its metabolites.

Methodology

Homology modeling

The non-availability of the 3D crystal structures of glutamate-cysteine ligase in the protein data bank hinder the direct investigation of GCL through *in silico* approach. Thus, the modeling of the structure from different organisms was carried out. The human and mouse primary sequence of glutamate-cysteine ligase (GCL) with respective accession number ID: A0A2R8YEL6 and Q3UNA7 were retrieved from UniProt knowledgebase (UniProtKB) (https://www.uniprot.org/) [10]. These obtained primary sequences were used in the prediction of the secondary structures of GCL using the SOPMA webserver (https://npsa-prabi.ibcp.fr/cgi-bin/npsa_automat.pl?page=/NPSA/npsa_sopma.html) [11]. However, the 3-dimensional structures of GCL were modeled using Swiss model webserver (https://swissmodel.expasy.org/interactive/) [12]. Two models were obtained for human and mouse GCLs, ranked and best obtained using their Z scores (-3.88 and -3.72 for human and mouse respectively) and the GMQE from the Swiss model results (Table 2). The best foreseen GCL models among the two models in human and mouse (model 1) were refined once through the $3D^{refine}$ web server to improve the quality of the protein (http://sysbio.rnet.missouri.edu/3Drefine/) [13-15]. There were five refined models obtained for each input respective 3D structures of GCL. The online PROCHECK webserver (https://saves.mbi.ucla.edu/) [16, 17] and Qualitative Model Energy Analysis (QMEAN) Swiss Model server (https://swissmodel.expasy.org/qmean/) [18] were used for the structural authentication and characterization of the five refined modeled GCLs for each organism source via the Ramachandran plot, verify 3D and RMS distances from planarity; and QMEAN Version 4.1.0 respectively to obtained the best model for each GCL organism models. In addition to the authentication of the GCL 3D structures, the ligand-binding sites of the best characterized refined models (the highest Ramachandran plot percentage) for each organism were scrutinized using COFACTOR (https://zhanglab.ccmb.med.umich.edu/COFACTOR/) [19].

In silico study

Ligand and protein molecule preparation

The SDF structures of naphthalene, 1-nitronaphthalene, 1-methylnaphthalene, 1,4-naphthoquinone, 1,2-naphthoquinone, naphthalene epoxide, glutathione with respective CIDs 931, 6849, 7002, 8530, 10667, 108063 and 124886 were retrieved from the PubChem database (www.pubchem.ncbi.nlm.nih.gov) [20]. The compounds were loaded on PyRx-Python Prescription 0.8 and converted to mol2 chemical format using Open babel [21]. All these compounds were selected individually, reduced energetically and autodocked to pdbqt format. The best characterized refined models of GCL for the three organisms: human glutamate-cysteine ligase (HGCL), and mouse glutamate-cysteine ligase (MGCL) were prepared individually for molecular docking. Each characterized refined 3D model was loaded on PyRx-Python Prescription 0.8, made molecule and converted to pdbqt format.

Molecular docking

The docking of the selected ligands to the best characterized refined GCL models and determination of binding affinities was carried out using PyRx-Python prescription 0.8 autodock vina tool [22]. Each autodocked model was selected with a single ligand at a time and run using blind docking approach and repeated for all ligands towards each model. The dimensions were set as grid center: x = -0.5583, y = 36.2078, z = -23.5008 for HGCL and x = 1.2726, y = 35.8790, z = -23.3508 for MGCL, with the grid size x = 65.2874, y = 67.1276, z = 73.0739 for HGCL and x = 80.3407, y = 76.7057, z = 71.5745 for MGCL. The first three ranking binding score results for all the ligands towards each GCL model obtained were selected and subjected to statistical analysis to see any significant difference among the GCL model-ligand interactions. The obtained statistical results were expressed as mean ± standard deviation of three determinations, analyzed using one-way analysis of variance (ANOVA) for mean differences between different ligands followed by Duncan post hoc correlation. The obtained autodocked files for all the ligands and the respective autodocked GCL models were visualized using Discovery Studio BIOVIA 2020 and the interaction views presented in 2D and 3D.

Results and discussion

Glutathione (GSH) is an indispensable and versatile metabolic tripeptide nonprotein thiol antioxidant in animal cells. It plays a significant role in metabolism, amino acid transport, and protection of the cell from reactive species and endogenous and exogenous toxic molecules [23]. Seelig *et al*. [24] and Chen *et al*. [25] reported the feedback

inhibition mechanism of GSH and adenosine triphosphate (ATP) on GCL via its smaller regulatory subunit [26]. The UniProt sequence analysis revealed that HGCL and MGCL contain 639 and 637 amino acid residues respectively (Figure 1). The result of the predicted secondary structure (Table 1 and Figures 2, 3 and 4) revealed the repetitive arrangements in space of adjacent amino acid residues in the GCL [27]. Also, the predicted secondary structure results showed that the proteins exist in four states namely; α-helix, random coil, extended strand and beta turn for both human and mouse. The percentage formation of these four states are respectively 41.94, 40.53, 12.99 and 4.54 for human; and 41.29, 40.82, 12.72 and 5.18 for mouse suggesting a better description of protein residues alignment [28] as well as better stability of the protein due to high degree of coil formation [27]. The swiss models (model 1 which had the highest scores) for respective human and mouse with GMQE and QMEAN scores 0.75 and -3.88 respectively and 0.76 and -3.72 respectively using *Saccharomyces cerevisiae* GCL (PDB ID: 3IG5; resolution 2.10 Å) as template were used for the modeling (Table 2, Figure 5). These closest respective GMQE, QMEANDisco (between 0 and 1) and QMEAN Z-score (between -4.0 and 0) values for human and mouse GCL models suggested a good quality, reliability and the degree of nativeness of the built models to the experimental structure of similar size [18, 29, 30]. In addition to the model quality result, the percentage sequence identity matrix for GCL model 1 are 44.76% and 45.67% for human and mouse respectively confirming the sequence similarity of GCL 1 models. The plot of the predicted local similarity to target against the residue number of the predicted 3D model structure (Figure 5) depicted a good estimate of local quality of the residues of the predicted model since most of the residues values are above 0.6 [31, 32]. The good quality of the predicted models was substantiated with the graphical plot of normalized QMEAN4 score against the protein size revealing the comparison with non-redundant set of PDB structures. The comparison result relates the quality scores of the predicted model to the obtainable scores for the experimental structure of like size suggesting a normalized QMEAN4 score of a standard deviation of the mean z score (|Z-score < 1). Interestingly, the $3D^{refined}$ models of GCLs showed an increased in the quality of the protein via Ramachandran plot using PROCHECK from 87.7% to 89.8% for human and from 89.1% to 89.6% (Table 3). The statistical result of the Ramachandran plots of the HGCL and MGCL amino acid residues revealed that (503 residues) 89.8% and (492 residues) 89.6% respectively are found in the favored region (A, B, and L; Red color), (51 residues) 9.1% and (50 residues) 9.1% respectively are found in the additional allowed region (a, b, l and p; yellow color), (3 residues) 0.5% and (4 residues) 0.7% respectively are found in the generously allowed region (~a, ~b, ~l, and ~p; light green and cream colors) and (3 residues) 0.5% and (3 residues) 0.5% respectively are found in the disallowed region (white color) (Figure 6). This result suggested that the phi and psi backbone dihedral

angles in both predicted structures of human and mouse GCL models are reasonably accurate [33]. The amino acid residues in the disallowed region are Glu168, Glu228 and Glu545 for human and Asn495, Asp499 and Glu543 for mouse. Furthermore, none of the planar atoms of the models has RMS distances that are not within the best fit plane with no black bars which indicate that all the residues of the models showed least deviation from the planarity (Figure 7). Remarkably, some of the residues (Phe, Trp and Tyr) of MGCL are off the graph [16, 17, 34, 35]. Captivatingly, the verify 3D revealed 85.49% and 88.85% (greater than 80%) of respective HGCL and MGCL amino acid residues had averaged 3D-1D score >= 0.2 (Figure 8). This results suggested that the two models (HGCL and MGCL) had a valid protein structure [36, 37]. Similarly, the result of the binding site identification (COFACTOR) corresponds to the 3D swiss model structure prediction for HGCL and MGCL models where *Saccharomyces cerevisiae* (3ig5) was used as the preferred template due to its GMQE values. In addition, Table 4a depicted the top 10 structural aligned (TM-align) identified analogs in PDB through the TM-score where values close to 1 indicate closed aligned sequence with least RMSD (low level of deviation among the amino acid residues) and high IDEN value (percentage similarity of the sequence) suggesting a moderately and reasonable model with good binding prediction [38]. Although both models (HGCL and MGCL) showed closed similarity with 3ig5, comparing the two predicted refined models, MGCL showed better TM-align prediction using TM-score, RMSD, IDEN and cov as analysis parameters [38]. It is evident from Table 4b that the predicted models are reliable with top five known enzymes homolog in PDB where 3ig5 identified as the topmost known enzyme with the highest confidence score $Cscore^{EC}$ values (0.191 and 0.199 for HGCL and MGCL respectively) for the enzyme commission number prediction. Similarly, the obtained result of the binding site score (BS-score) prediction showed that both predicted models for different ligands as seen in the BS-score values which are approximately equal to 1 or above suggest a realistic local binding match between the predicted models and the templates (Table 4c) [38]. In this binding site prediction analysis, HGCL showed perfect local binding match to two templates (3lvvA) with BS-score values 1.62 and 1.50 and moderate local binding match to three templates: 2gwdA, 3o6xA and 2d32D with respective BS-score values 0.99, 0.90 and 0.86 while MGCL depicted absolute perfect local binding match to all the top four templates used with BS-score values greater than 1 in all the ligands such as glutamate (Glu), glutathione (GSH), adenosine diphosphate (ADP) and Magnesium (Mg). In almost similar pattern, the predicted gene ontology results via molecular function, biological processes and cellular part reveals accurate and reliable data for the predicted models with all confidence score for gene ontology ($Cscore^{GO}$) values greater 0.5 (Table 4d) [38].

Figure 1. The primary sequence of human glutamate-Cysteine ligase (HGCL) and mouse glutamate-Cysteine ligase (GCL).

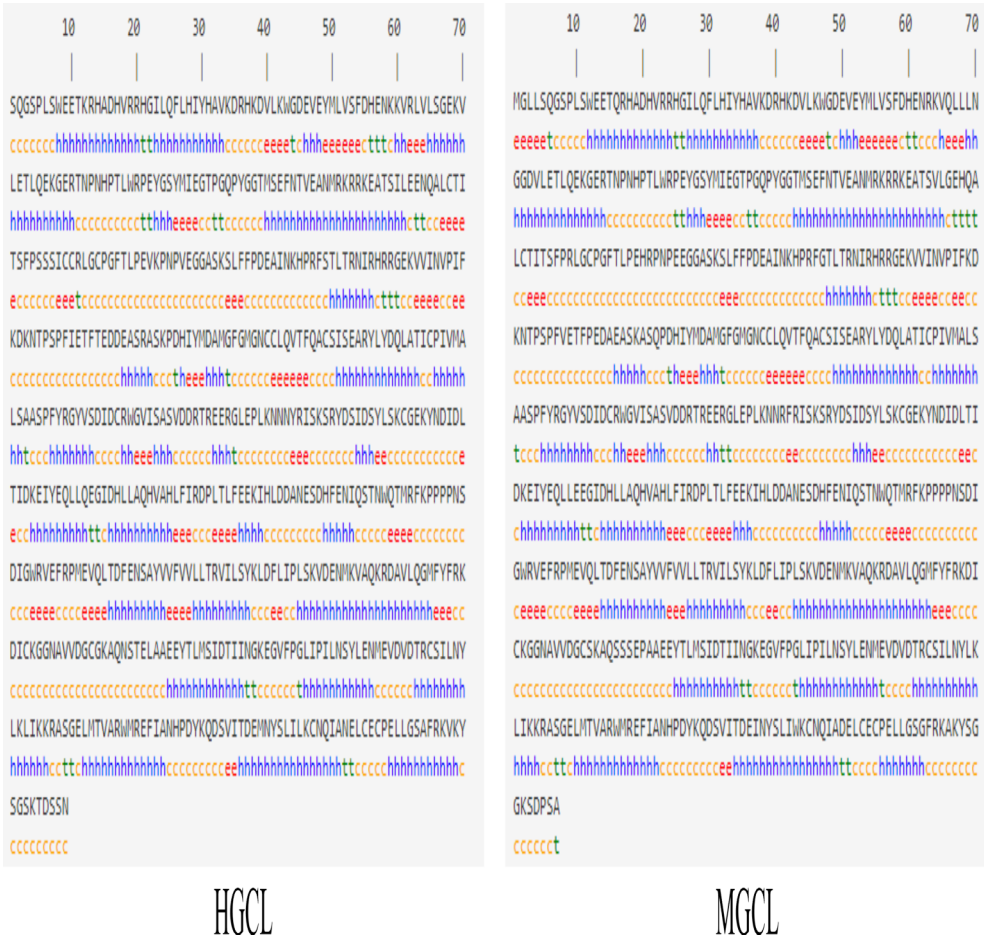

Figure 2. The SOPMA secondary sequence prediction of glutamate-cysteine ligase from human (HGCL), and mouse (MGCL).

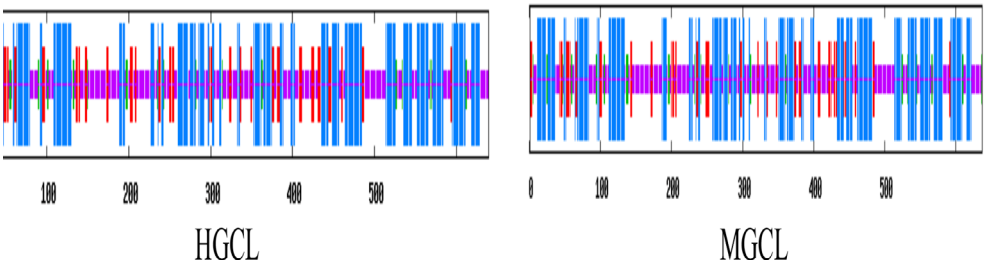

Figure 3. The SOPMA secondary structure types for glutamate-cysteine ligase from human (HGCL) and mouse (MGCL).

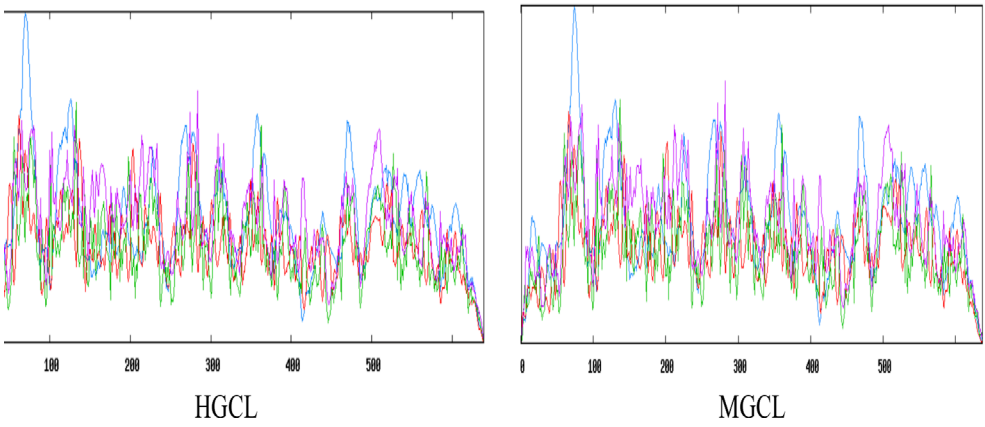

Figure 4. The SOPMA secondary structure states of glutamate-cysteine ligase from human (HGCL), and mouse (MGCL).

Table 1. The predicted SOPMA secondary structures of glutamate-cysteine ligase and sequence length from human and mouse.

Source	Human	Mouse
Sequence length	639	637
SOPMA Secondary Predicted Structure (%)		
Alpha helix (Hh)	(268) 41.94	(263) 41.29
3_{10} helix (Gg)	(0) 0.00	(0) 0.00
Pi helix (Ii)	(0) 0.00	(0) 0.00
Beta bridge (Bb)	(0) 0.00	(0) 0.00
Extended strand (Ee)	(83) 12.99	(81) 12.72
Beta turn (Tt)	(29) 4.54	(33) 5.18
Bend region (Ss)	(0) 0.00	(0) 0.00
Random coil (Cc)	(259) 40.53	(260) 40.82
Ambiguous state (?)	(0) 0.00	(0) 0.00
Other states	(0) 0.00	(0) 0.00
Other parameters		
Windows width	17	17
Similarity threshold	8	8
Number of states	4	4

Table 2. The predicted 3D crystal Swiss models of glutamate-cysteine ligase from human and mouse.

Organism sources	Human			Mouse		
No of Models built	Model 1	Model 2	Model 3	Model 1	Model 2	Model 3
QMEAN Z-Scores	-3.88	-4.64	-2.80	-3.72	-4.85	-2.41
QMEANDisco	0.73±0.05	0.20±0.12	0.24±0.12	0.75±0.05	0.28±0.12	0.24±0.12
GMQE	0.75	0.00	0.00	0.76	0.00	0.00
Template	3ig5.1.A	2mfi.1.A	4r71.2.C	3ig5.1.A	2mfi.1.A	4r71.2.C
Sequence Similarity	0.41	0.28	0.30	0.42	0.27	0.29
Sequence Identity	44.76%	21.62%	23.33%	45.67%	19.44%	20.00%

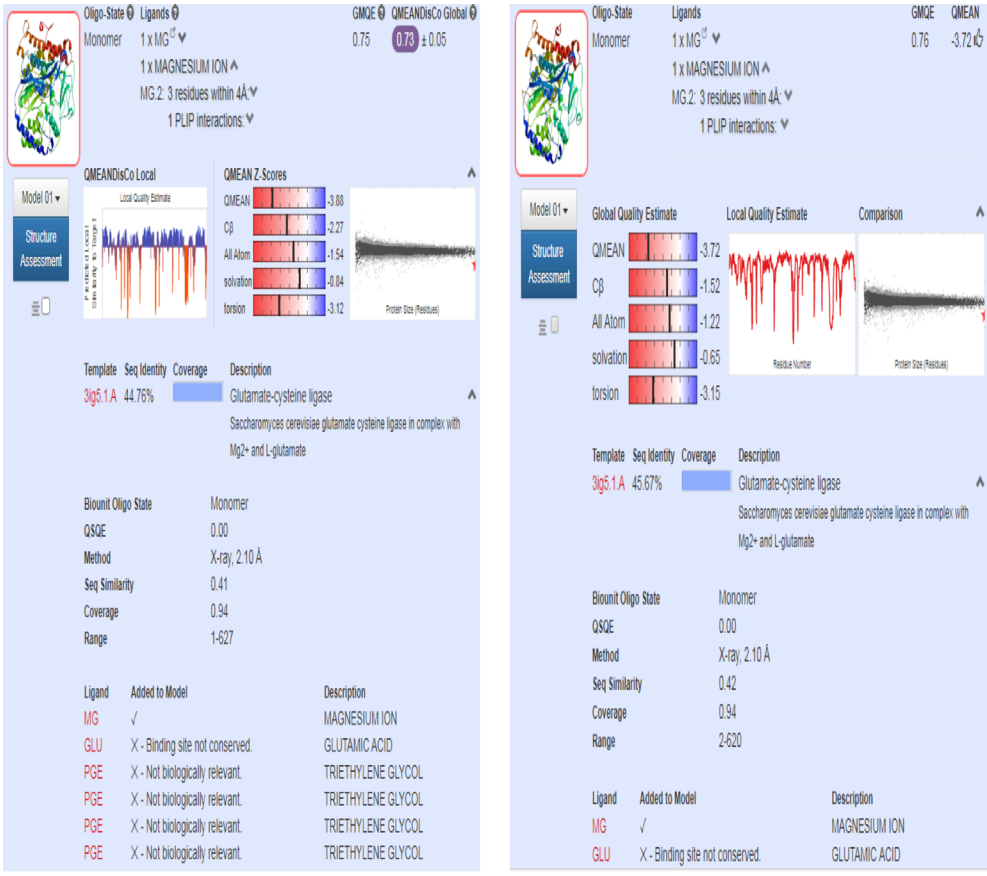

Figure 5. The refined swiss model 3D crystal structures of glutamate-cysteine ligase from human and mouse.

Table 3. The PROCHECK Ramachandran plots of the chosen refined Swiss model 3D crystal structures.

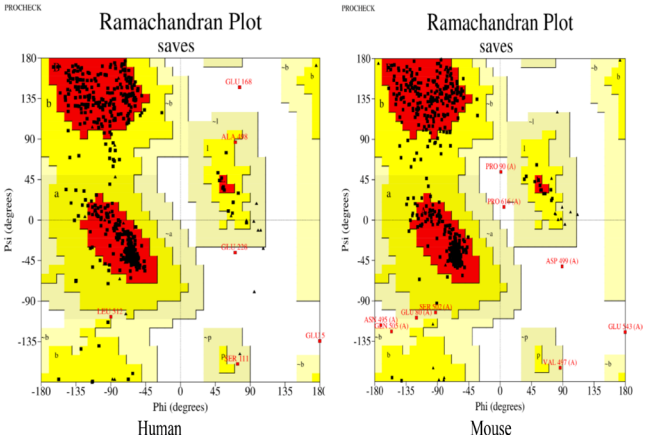

Figure 6. The PROCHECK Ramachandran plots of refined HGCL and MGCL models.

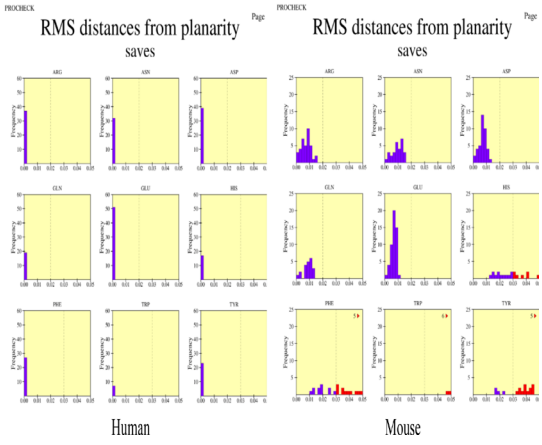

Figure 7. The PROCHECK RMS distances from planarity of HGCL, and MGCL models.

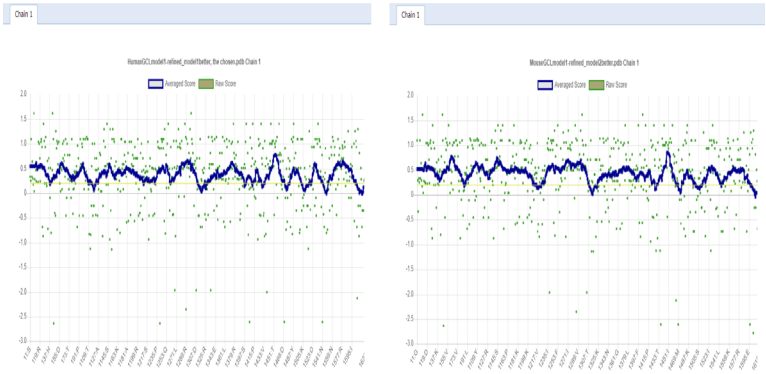

Figure 8. The PROCHECK verify 3D of HGCL and MGCL models.

Molecular docking study

To substantiate the homology modeling assessment of the predicted GCL 3D crystal structure models, the molecular docking done using naphthalene and its metabolites as ligands in reference to a known inhibitor (GSH). The binding scores, interacting residues were obtained as well as the type of non-covalent interactions between the respective ligand towards the GCL models are shown in Tables 5a and 5b, and Figures 9a and 9b. The molecular docking binding scores for all the ligands examined towards HGCL were all significantly different and showed better binding scores than GSH (binding score -5.20±0.00 kcal/mol). Although GSH interacted mostly with HGCL via conventional hydrogen bond compared to assessed ligands as proposed by Elokely and Doerksen [39], the high binding score could be due to other non-covalent interactions mostly pi-interaction orientations such as pi-pi stacked, pi-pi T-shaped and pi-sigma with residues like Phe210, Val292, Arg580, Ala584 (Table 5a and Figure 9a). All the assessed ligands interacted with HGCL in a different pocket compared to GSH which could be responsible for their significant better binding scores arose from different non-covalent interactions other than covalent hydrogen bond as seen in GSH. These pi-interactions, which are not affected by solvation/desolvation could contribute to the inhibition binding from the assessed ligands [40, 41]. Similarly, MGCL molecular docking binding scores followed almost the same pattern in which all the assessed ligands had better binding scores than GSH. Also, the interactions are mainly non-covalent interactions with no conventional hydrogen bond interaction among the ligands except 1,2-naphthoquinone (CID: 10667) where Lys46 hydrogen bond interaction was observed. Conversely, MGCL ligand binding occurred in two different pockets: pocket 1 with residues mainly Phe383, Lys386 and Asp396 while the main residues that interacted in pocket 2 are Lys46 and Pro109

Table 4a. TM-align identified top 10 structural analogs in PDB.

Rank	PDB Hit	HGCL				MGCL			
		TM-Score	RSMD[a]	IDEN[a]	Cov	TM-Score	RSMD[a]	IDEN[a]	Cov
1	3ig5A	0.94	1.18	0.438	0.957	0.96	1.12	0.450	0.966
2	2gwcF	0.55	3.14	0.135	0.608	0.56	3.10	0.132	0.616
3	2d33A	0.52	4.35	0.086	0.614	0.52	4.37	0.092	0.622
4	1r8gB	0.51	2.59	0.133	0.550	0.52	2.53	0.136	0.557
5	3nztA	0.51	4.13	0.090	0.601	0.52	4.19	0.086	0.611
6	3ln7A	0.49	4.01	0.094	0.571	0.49	3.97	0.090	0.577
7	3ln6A1	0.32	3.58	0.101	0.359	0.32	3.58	0.100	0.363
8	4jzaA	0.30	8.27	0.041	0.502	0.30	8.22	0.025	0.512
9	3lmmD	0.23	7.88	0.036	0.368	0.24	7.55	0.050	0.373
10	3g7rB	0.20	5.32	0.080	0.258	0.20	5.29	0.081	0.262

(a) Ranking of proteins is based on TM-score of the structural alignment between the query structure and known structures in the PDB library. (b) RMSD[a] is the RMSD between residues that are structurally aligned by TM-align. (c) IDEN[a] is the percentage sequence identity in the structurally aligned region. (d) Cov. represents the coverage of the alignment by TM-align and is equal to the number of structurally aligned residues divided by length of the query protein.

Table 4b. Top 5 enzyme homologs in PDB.

Rank	HGCL					MGCL				
	PDB Hit	Cscore[EC]	TM-Score	RSMD[a]	IDEN[a]	PDB Hit	Cscore[EC]	TM-Score	RSMD[a]	IDEN[a]
1	3ig5A	0.191	0.944	1.18	0.438	3ig5A	0.199	0.958	1.12	0.450
2	2gwdA	0.083	0.569	3.20	0.131	2gwdA	0.090	0.577	3.18	0.128
3	2d33A	0.066	0.517	4.35	0.086	3nztA	0.066	0.518	4.19	0.086
4	1pj6A	0.060	0.322	8.32	0.051	2d33A	0.066	0.523	4.37	0.092
5	1b0pA	0.060	0.341	8.24	0.050	1pj6A	0.060	0.326	7.59	0.034

(a) Cscore[EC] is the confidence score for the Enzyme Commission (EC) number prediction with values ranging between [0-1]; where a higher score indicates a more reliable EC number prediction. (b) TM-score is a measure of global structural similarity between query and template protein. (c) RMSD[a] is the RMSD between residues that are structurally aligned by TM-align. (d) IDEN[a] is the percentage sequence identity in the structurally aligned region.

Table 4c. Template proteins with similar binding site.

Rank	HGCL					MGCL				
	PDB Hit	$Cscore^{LB}$	TM-Score	BS-score	Ligand Name	PDB Hit	$Cscore^{LB}$	TM-Score	BS-score	Ligand Name
1	3lvvA	0.44	0.946	1.62	LBP	3ig5A	0.49	0.959	1.61	Glu
2	3lvvA	0.28	0.946	1.50	ADP	3lvwA	0.32	0.959	1.67	GSH
3	2gwdA	0.10	0.569	0.99	Glu	3ig8A	0.29	0.959	1.49	ADP
4	3o6xA	0.02	0.391	0.90	Mg	3o6xA	0.04	0.395	1.07	Mg
5	2d32D	0.02	0.513	0.86	Cys					

(a) $Cscore^{LB}$ is the confidence score of predicted binding site with values ranging between [0-1]; where a higher score indicates a more reliable ligand-binding site prediction. (b) BS-score is a measure of local similarity (sequence & structure) between template binding site and predicted binding site in the query structure. Based on large scale benchmarking analysis, we have observed that a BS-score >1 reflects a significant local match between the predicted and template binding site. (c) TM-score is a measure of global structural similarity between query and template protein.

Table 4d. Predicted gene ontology for the refined GCL models via molecular function, biological process and cellular components.

Cofactor parameters	HGCL			MGCL		
	GO term	$Cscore^{GO}$	Name	GO term	$Cscore^{GO}$	Name
Molecular Function	GO: 0004357	1.00	GCL activity	GO: 0004357	1.00	GCL activity
Biological Process	GO: 0006750	1.00	glutathione biosynthetic process	GO: 0006750	1.00	glutathione biosynthetic process
	GO: 0044699	0.55	Single-organism process	GO: 0044699	0.51	Single-organism process
Cellular Component	GO: 0044424	1.00	Intracellular part	GO: 0044424	1.00	Intracellular part
	GO: 0044444	0.95	Cytoplasmic part	GO: 0044444	0.94	Cytoplasmic part
	GO: 0043234	0.91	Protein complex	GO: 0017109	0.90	GCL complex
	GO: 0017109	0.90	GCL complex			

Table 5a. Molecular docking binding scores of naphthalene and its metabolites towards HGCL and the non-covalent interacting residues.

Parameters / Ligand CID	Binding score (kcal/mol)	HGCL non-covalent interacting residues									
		Conventional H- bond	Alkyl	Amide - Pi Stacked	C-H bond	Pi - Alkyl	Pi-Donor H-bond	Pi - Pi Stacked	Pi - Sigma	Pi-Pi T-Shaped	Unfavorable Donor-Donor
931	-6.07±0.12^{bc}					Pro86, Met110				Tyr106	
6849	-6.20±0.00^{ab}					Val292, Arg580		Phe210	Ala584		
7002	-6.27±0.06^{a}		Phe210, Arg580	Ile583		Val292, Arg580, Ala584		Phe210	Ala584		
8530	-6.00±0.00^{cd}	Thr436						Phe438	Leu563		
10667	-6.17±0.12^{abc}	Pro86, Asn119				Pro86	Glu104	Tyr106			
108063	-5.83±0.21^{d}		Pro86, Tyr106		Asn114	Met110					
124886	-5.20±0.00^{e}	Glu92, Glu99, Arg187, Asn402, Ser405, Arg429			Ser405						Arg187

Table 5b. Molecular docking binding scores of naphthalene and its metabolites towards MGCL and the non-covalent interacting residues.

Parameters / Ligand CID	Binding score (Kcal/mol)	MGCL non-covalent interacting residues						
		Conventional H- bond	C-H bond	Pi-Alkyl	Pi-Anion	Pi-Cation	Pi-Sigma	Pi-Pi T-Shaped
931	-5.80±0.00[bc]			Phe383	Asp396	Lys386		Phe383
6849	-6.27±0.06[ab]			Phe383		Lys386		Phe383
7002	-6.07±0.12[bc]			Phe383	Asp396	Lys386		Phe383
8530	-6.33±0.12[ab]		Thr253	Lys46, Pro109, Arg423			Pro109	
10667	-6.67±0.15[a]	Lys46	Trp47				Pro109	
108063	-5.90±0.10[bc]			Phe383	Asp396	Lys386		Phe383
124886	-5.67±0.72[c]	Lys46, Asp49, Thr253	Gly48, Thr253					

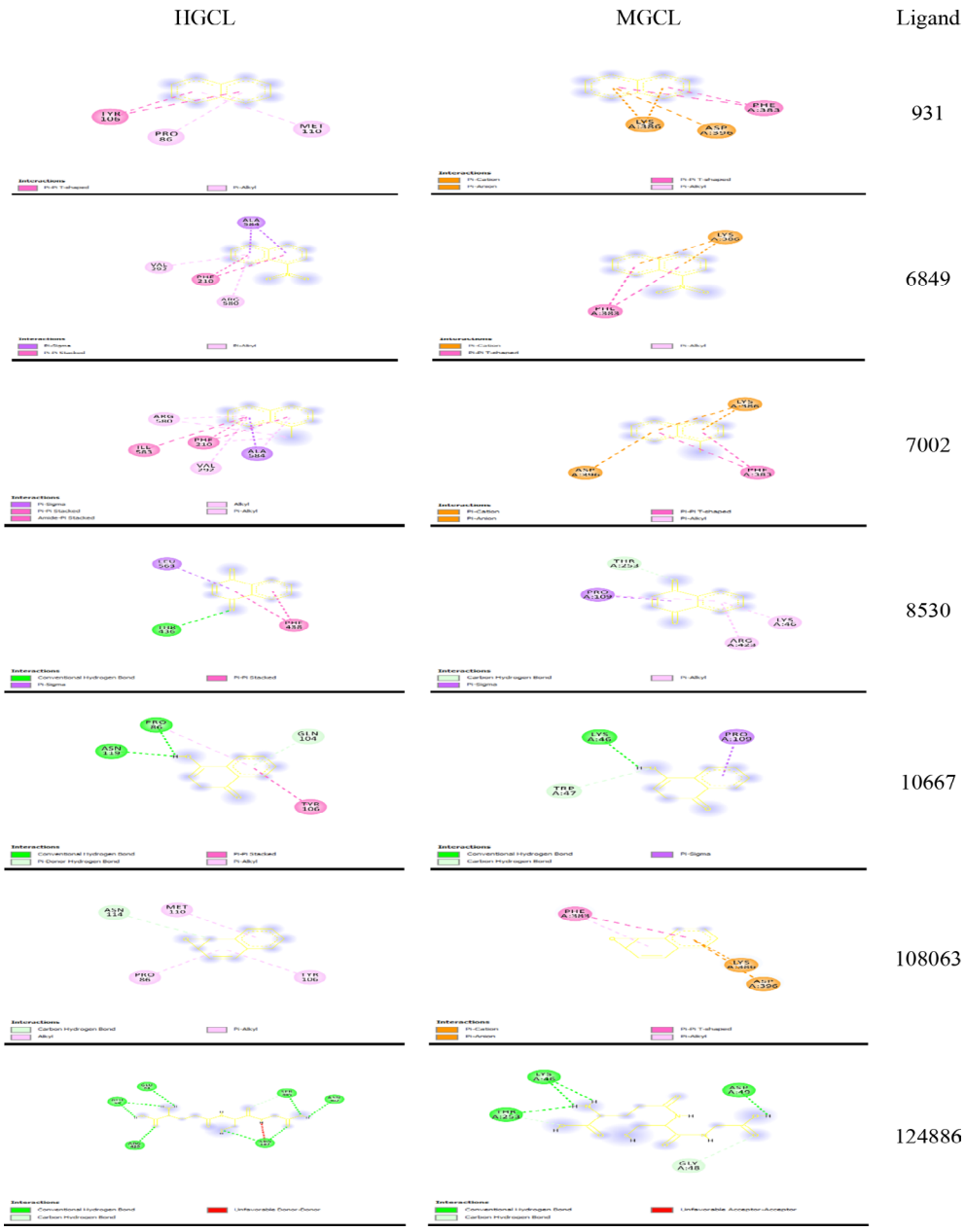

Figure 9a. 2D molecular binding structures of HGCL, and MGCL with 931 (naphthalene), 6849 (1-nitronaphthalene), 7002 (1-methynaphthalene), 8530 (1,4-naphthoquinone), 10667 (1,2-naphthoquinone), 108063 (naphthalene epoxide), and 124886 (glutathione).

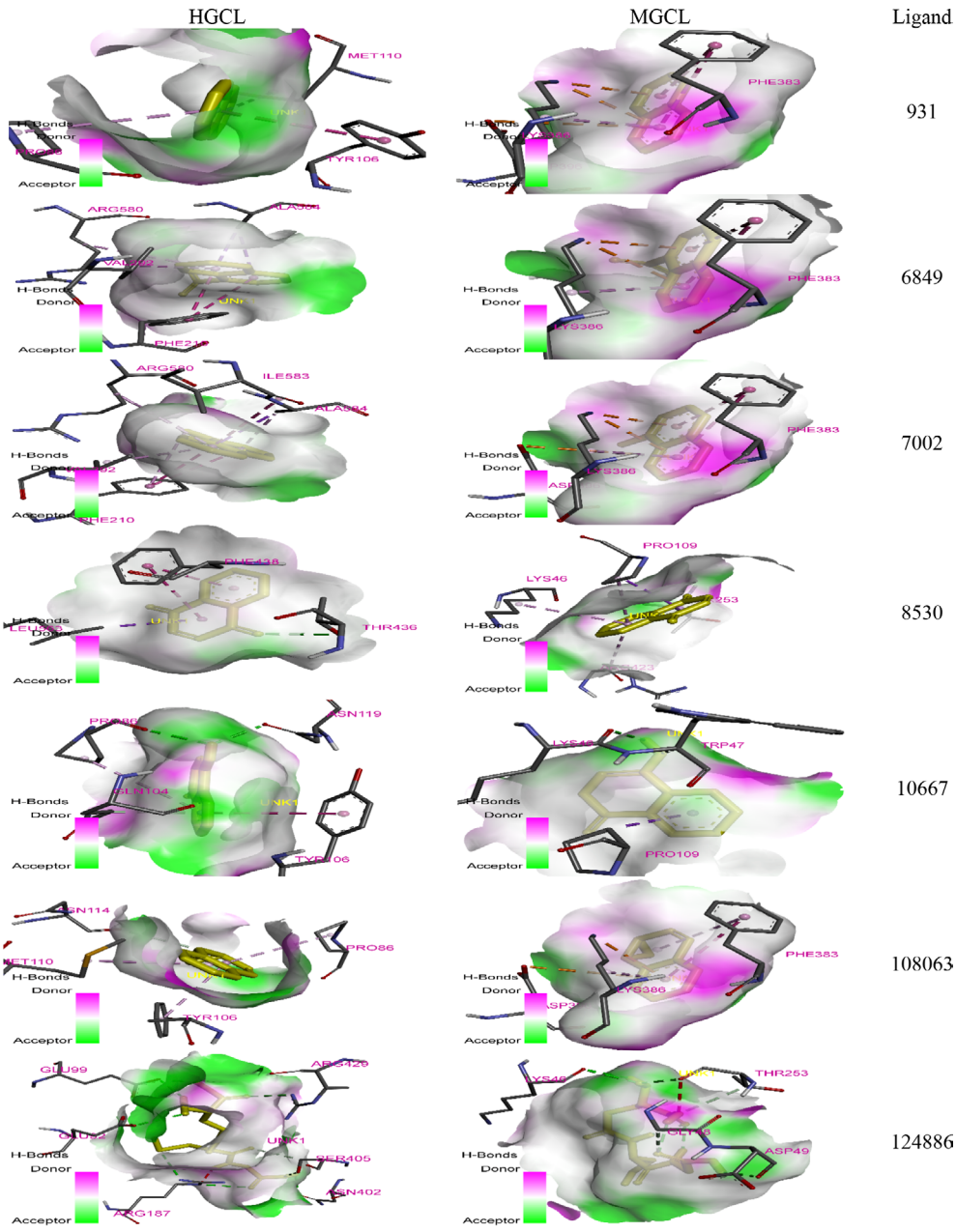

Figure 9b. 3D molecular binding structures of HGCL, and MGCL with 931 (naphthalene), 6849 (1-nitronaphthalene), 7002 (1-methynaphthalene), 8530 (1,4-naphthoquinone), 10667 (1,2-naphthoquinone), 108063 (naphthalene epoxide), and 124886 (glutathione).

Conclusion

Considering the fact that GCL is essential in the de novo synthesis of GSH, the assessment of HGCL and MGCL provides considerable catalytic mechanism and suggests approaches through which inhibitors with higher binding affinity may be attained the proposed revealed binding sites could be preserved. To the best of our knowledge, the study has revealed different binding pockets for the two models that could influence the physico-chemical properties of ligand binding interactions with the enzyme needed for effective *in silico* GCL inhibitor designing.

Acknowledgements

The support provided by the staff of Department Biochemistry, College of Natural and Applied Sciences, McPherson University, Seriki Sotayo, Ogun State, Nigeria is well appreciated.

Disclosure statement

The authors declare that they have no conflict of interest.

References

1. C. Espinosa-Diez, V. Miguel, D. Mennerich, T. Kietzmann, P. Sanchez-Perez, S. Cadenas, S. Lamas, Antioxidant responses and cellular adjustments to oxidative stress, *Redox Biol.*, **6**, 183-197 (2015).

2. T.P. Dalton, Y. Chen, S.N. Schneider, D.W. Nebert, H.G. Shertzer, Genetically altered mice to evaluate glutathione homeostasis in health and disease, *Free Radic. Biol. Med.*, **37**, 1511-1526 (2004).

3. D. Morris, J. Ly, P.-T. Chi, J. Daliva, T. Nguyen, C. Soofer, Y.C. Chen, M. Lagman, V. Venketaraman, Glutathione synthesis is compromised in erythrocytes from individuals with HIV, *Front. Pharmacol.*, **5**, 73 (2014).

4. Y. Yang, M.Z. Dieter, Y. Chen, H.G. Shertzer, D.W. Nebert, T.P. Dalton, Initial characterization of the glutamate-cysteine ligase modifier subunit Gclm(-/-) knockout mouse. Novel model system for a severely compromised oxidative stress response, *J. Biol. Chem.*, **277**, 49446-49452 (2002).

5. C.C. Franklin, D.S. Backos, I. Mohar, C.C. White, H.J. Forman, T.J. Kavanagh, Structure, function, and post-translational regulation of the catalytic and modifier subunits of glutamate cysteine ligase, *Mol. Aspects Med.*, **30**, 86-98 (2009).

6. N. Fu, D. Li, W. Li, W. Zhao, S. Zhang, L. Liu, S. Zhao, J. Du, L. Kong, R. Wang, Y. Zhang, Y. Nan, Glutamate-cysteine ligase catalytic subunit attenuated hepatitis C virus-related liver fibrosis and suppressed endoplasmic reticulum stress, *Front. Mol. Biosci.*, **7**, 199 (2020).

7. Y. Xiong, Y. Xiong, Y. Wang, Z. Wang, A. Zhang, N. Zhao, D. Zhao, Z. Yu, Z. Wang, J. Yi, X. Luan, Inhibition of glutathione synthesis via decreased glucose metabolism in stored RBCs, *Cell. Physiol. Biochem.*, **51**, 2172-2184 (2018).

8. Y. Kumagai, Y. Abiko, Environmental electrophiles: Protein adducts, modulation of redox signaling, and interaction with persulfides/polysulfides, *Chem. Res. Toxicol.*, **30**, 203-219 (2017).

9. R.M. Baldwin, W.T. Jewell, M.V. Fanucchi, C.G. Plopper, A.R. Buckpitt, Comparison of pulmonary/nasal CYP2F expression levels in rodents and rhesus macaque, *J. Pharmacol. Exp. Therapy*, **309**, 127-136 (2004).

10. The UniProt Consortium, UniProt: the universal protein knowledgebase in 2021, *Nucleic Acids Research* **49** (D1) (2021) D480-D489. URL: https://doi.org/10.1093/nar/gkaa1100

11. C. Combet, C. Blanchet, C. Geourjon, G. Deléage NPS@: Network protein sequence analysis, *Trends Biochem. Sci.*, **25**(3), 147-150 (2000).

12. A. Waterhouse, M. Bertoni, S. Bienert, G. Studer, G. Tauriello, R. Gumienny, FT. Heer, TAP. de Beer, C. Rempfer, L. Bordoli, R. Lepore, T. Schwede, SWISS-MODEL: homology modelling of protein structures and complexes, *Nucleic Acids Res.*, **46**(W1), W296-W303 (2018).

13. D. Bhattacharya, J. Cheng, 3Drefine: Consistent protein structure refinement by optimizing hydrogen bonding network and atomic level energy minimization, *Proteins: Structure, Function, and Bioinformatics*, **81**(1), 119-131 (2012).

14. D. Bhattacharya, J. Cheng, i3Drefine software for protein 3D structure refinement and its assessment in CASP10, *PLoS One*, **8**(7), e69648 (2013).

15. D. Bhattacharya, J. Nowotny, R. Cao, J. Cheng, 3Drefine: an interactive web server for efficient protein structure refinement, *Nucleic Acids Res.*, **44**(W1), W406-W409 (2016). doi: 10.1093/nar/gkw336.

16. R.A. Laskowski, M.W. MacArthur, D.S. Moss, J.M. Thornton, PROCHECK: a program to check the stereochemical quality of protein structures, *J. Appl. Crystal.*, **26**(2), 283-291 (1993).

17. R.A. Laskowski, J.A. Rullmannn, M.W. MacArthur, R. Kaptein, J.M. Thornton, AQUA and PROCHECK-NMR: programs for checking the quality of protein structures solved by NMR, *J. Biomol. NMR*, **8**(4), 477-486 (1996).

18. P. Benkert, M. Biasini, T. Schwede, Toward the estimation of the absolute quality of individual protein structure models, *Bioinformatics*, **27**(3), 343-350 (2011) 343-350.

19. A. Roy, J. Yang, Y. Zhang, COFACTOR: an accurate comparative algorithm for structure-based protein function annotation, *Nucleic Acids Res.*, **40**(W1), W471-W477 (2012).

20. S. Kim, J. Chen, T. Cheng, A. Gindulyte, J. He, S. He, Q. Li, B.A. Shoemaker, P.A. Thiessen, B. Yu, L. Zaslavsky, J. Zhang, E.E. Bolton, PubChem 2019 update: improved access to chemical data, *Nucleic Acids Res.*, **47**(D1), D1102–D1109 (2019).

21. N.M. O'Boyle, M. Banck, C.A. James, C. Morley, T. Vandermeersch, GR. Hutchison, Open Babel: An Open chemical toolbox, *J. Cheminformatics*, **3**(10), 33 (2011).

22. O. Trott, AJ. Olson, AutoDock Vina: Improving the speed and accuracy of docking with a new scoring function, efficient optimization and multithreading, *J. Comput. Chem.*, **31**(2), 455-461 (2010).

23. A. Meister, Glutathione metabolism and its selective modification, *J. Biol. Chem.*, **263**(33), 17205-17208 (1988).

24. G.F. Seelig, R.P. Simondsen, A. Meister, Reversible dissociation of gamma-glutamylcysteine synthetase into two subunits, *J. Biol. Chem.*, **259**, 9345-9347 (1984).

25. Y. Chen, H.G. Shertzer, S.N. Schneider, D.W. Nebert, T.P. Dalton, Glutamate cysteine ligase catalysis: Dependence on ATP and modifier subunit for regulation of tissue glutathione levels, *J. Biol. Chem.*, **280** 33766-33774 (2005).

26. CS. Huang, ME. Anderson, A. Meister, Amino acid sequence and function of the light subunit of rat kidney gamma-glutamylcysteine synthetase, *J. Biol. Chem.*, **268**, 20578-20583 (1993).

27. JM. Mason and KM. Arndt, Coiled coil domains: stability, specificity and biological implications, *ChemBioChem*, **5**(2), 170-176 (2004).

28. C. Geourjon, G. Deléage, SOPMA: significant improvements in protein secondary structure prediction by consensus prediction from multiple alignments, *Bioinformatics*, **11**(6), 681-684 (1995).

29. JM. Cardoso, L. Fonseca, C. Egas, I. Abrantes, Cysteine proteases secreted by the pinewood nematode, Bursaphelenchus xylophilus: in silico analysis, *Comput. Biol. Chem.*, **77,** 291-296 (2018).

30. B. Patel, V. Singh, D. Patel, Structural bioinformatics, in: N.A. Shaik, K.R. Hakeem, B. Banaganapalli, R. Elango (editors), *Essentials of Bioinformatics*, vol. I., Springer, Cham, Switzerland, 2019, pp. 169-199.

31. O.G. Oduselu, O.O. Ajani, U.Y. Ajamma1, B. Brors, E. Adebiyi, Homology modelling and molecular docking studies of selected substituted benzo[d]imidazol-1-yl)methyl) benzimidamide scaffolds on *Plasmodium falciparum* adenylosuccinate lyase receptor, *Bioinform. Biol. Insights*, **13,** 1177932219865533 (2019).

32. A.O. Roland, A.E. Morayo, O. Joan, F.I. Gbadamosi, E. Kayode, M. Adelabu, Modelling profile of onchocerca volvulus glutamate-cysteine ligase (ONCVO-GCL), *J. Anal. Pharm. Res.*, **10**(3), 118-122 (2021).

33. H. Yamaguchi, T. Akitaya, Y. Kidachi, K. Kamiie and H. Umetsu, Homology modeling and structural analysis of human γ-glutamylcysteine ligase catalytic subunit for antitumor drug development, *J. Biophys. Chem.*, **3**(3), 238-248 (2012)

34. A.L. Morris, M.W. MacArthur, E.G. Hutchinson, J.M. Thornton, Stereochemical quality of protein structure coordinates, *Proteins*, **12**, 345-364 (1992).

35. RA. Laskowski, MW. MacArthur, JM. Thornton, PROCHECK: validation of protein structure coordinates, in: M.G. Rossmann, E. Arnold (editors), *International Tables of Crystallography, Volume F. Crystallography of Biological Macromolecules*, Kluwer Academic Publishers, The Netherlands, 2001, pp. 722-725.

36. R. Lüthy, J.U. Bowie, D. Eisenberg, A method to identify protein sequences that fold into a known three-dimensional structure, *Science*, **253**(5016), 164-170 (1991).

37. R. Lüthy, J.U. Bowie, D. Eisenberg, Assessment of protein models with three-dimensional profiles, *Nature* **356**(6364), 83-85 (1992).

38. C. Zhang, P.L. Freddolino, Y. Zhang, COFACTOR: improved protein function prediction by combining structure, sequence and protein–protein interaction information, *Nucleic Acids Res.*, **45** (Web Server issue) W291-W299 (2017).

39. K.M. Elokely, R.J. Doerkse, Docking challenge: protein sampling and molecular docking performance, *J. Chem. Inform. Model.*, **53**(8), 1934-1945 (2013).

40. M.J.A. Bernaldez, J.B. Billones, A. Magpantay, In silico analysis of binding interactions between GSK983 and Human DHODH through docking and molecular dynamics, *AIP Conference Proceedings*, **2045**, 020073 (2018).

41. I. Olaoye, B. Oso, A. Aberuagba, Molecular mechanisms of anti-inflammatory activities of the extracts of *Ocimum gratissimum* and *Thymus vulgaris*, *Avicenna Journal of Medical Biotechnology*, **13**(4), 207-216 (2021).

How to cite this article

I. Olaoye, B. Oso, A. Aberuagba, Molecular insights into the binding mechanisms of human and mouse Glutamate-cysteine ligases, *Rev. Colomb. Cienc. Quim. Farm.*, **52**(1), 311-336 (2023). https://doi.org/10.15446/rcciquifa.v52n1.109381